RSC Advances

PAPER

View Article Online
View Journal | View Issue

Check for updates

Cite this: *RSC Adv.*, 2022, **12**, 17682

Synthesis and photophysical properties of *N*-alkyl dithieno[3,2-*b*:2′,3′-*d*]pyrrole based donor/acceptor-π-conjugated copolymers for solar-cell application†

Cuc Kim Trinh, ‡*[a] Gamal M. Nassar,‡[bc] Nabiha I. Abdo,[d] Suhyun Jung,[b] Wonbin Kim,[b] Kwanghee Lee[b] and Jae-Suk Lee *[b]

Two kinds of donor–acceptor π-conjugated copolymer based on poly{[*N*-hexyl-dithieno(3,2-*b*:2′,3′-*d*)pyrrole-2,6-diyl]*alt*-[isoindigo]} (PDTP-IID) and poly{[*N*-hexyl-dithieno(3,2-*b*:2′,3′-*d*)pyrrole-2,6-diyl]*alt*-[thiazol-2,5-diyl]} (PDTP-Thz) were investigated. These copolymers were synthesized *via* a Stille coupling reaction. The results showed the structure–property relationships of different donor–acceptor (D–A) combinations. The polymer structures and photophysical properties were characterized by ^{1}H NMR, TGA, DSC, UV-vis absorption spectroscopy, AFM, CV, and XRD measurement. Through UV-vis absorption and cyclic voltammetry (CV) measurements, it showed that the copolymers exhibit not only a low bandgap of 1.29 eV and 1.51 eV but also a deep highest occupied molecular orbital (HOMO) of −5.49 and −5.11 eV. Moreover, photovoltaic properties in combination with the fullerene derivatives were investigated. The device based on the copolymers with $PC_{71}BM$ exhibited higher maximum power conversion efficiency and higher maximum short-circuit current density of 0.23% with 1.64 mA cm^{-2} of PDTP-IID:$PC_{71}BM$ and 0.13% with 1.11 mA cm^{-2} of PDTP-Thz:$PC_{71}BM$ than those of the copolymers with $PC_{61}BM$. Measurements performed for *N*-hexyl-dithieno(3,2-*b*:2′,3′-*d*)pyrrole-based copolymers proved the potential of these polymers to be applied in optoelectronic applications.

Received 24th April 2022
Accepted 23rd May 2022

DOI: 10.1039/d2ra02608b

rsc.li/rsc-advances

Open Access Article. Published on 15 June 2022. Downloaded on 2/7/2026 12:35:11 PM.
This article is licensed under a Creative Commons Attribution-NonCommercial 3.0 Unported Licence.

Introduction

Bulk heterojunction (BHJ) organic solar cells based on conjugated p-type polymers and n-type fullerene derivatives generally function as electron donors and acceptors and have been investigated due to their advantages of low cost, light weight, *etc.*[1–4] These bulk-heterojunction (BHJ) organic solar cells offer the advantages of easier fabrication with higher conversion efficiency due to the considerably extended donor/acceptor interface. After many years, some basic rules for solar cell applications have come out for designing an efficient p-type material such as a low bandgap, a deep highest occupied molecular orbital (HOMO) to exhibit high open-circuit voltage, high hole mobility for efficient charge transport and good solubility in common solvents for device fabrication processing.[5–7] Therefore, many research groups have designed and analyzed new π-conjugated organic semiconductors in the past decades.

Dithieno[3,2-*b*:2′,3′-*d*]pyrrole (DTP) is one of the most attractive building blocks for materials in organic solar cell devices. It has a completely flat crystal structure with good π-conjugation and better solubility without changing the planarity. In addition, the nitrogen atom in dithieno[3,2-*b*:2′,3′-*d*]pyrroles molecule enhances the ability of electron-donating. However, some poly(*N*-alkyl dithieno[3,2-*b*:2′,3′-*d*]pyrroles) have low solubility which is the major obstacle to their use in devices. Many scientists have been studying to improve the solubility of the polymers by increasing the length of the alkyl chain attaching to the N-atom or incorporating substituted donor or acceptor units containing the alkyl chains into the polymer backbone.[8,9] A series of copolymers based on DTP and various acceptors were investigated in fullerene-based organic solar cells.[10–14] However, their obtained PCEs are below 4% with poor open-circuit voltage (V_{OC}), short-circuit density (J_{SC}), and fill factor (FF). These results may come from the high-lying HOMO energy levels and limited light absorption, as well as the poor morphology of the blend active layer.

To overcome these limitations, many research groups have focused on improving the light absorption ability and band

[a]*Chemical Engineering in Advanced Materials and Renewable Energy Research Group, School of Engineering and Technology, Van Lang University, Ho Chi Minh City, Vietnam. E-mail: cuc.tk@vlu.edu.vn*

[b]*School of Materials Science & Engineering, Gwangju Institute of Science and Technology (GIST), Gwangju 61005, Republic of Korea. E-mail: jslee@gist.ac.kr*

[c]*Department of Chemistry, Faculty of Science, Tanta University, Tanta 31527, Egypt*

[d]*Higher Institute of Engineering and Technology, New Borg Al Arab, Alexandria, Egypt*

† Electronic supplementary information (ESI) available. See https://doi.org/10.1039/d2ra02608b

‡ Contributed equally to this work.

© 2022 The Author(s). Published by the Royal Society of Chemistry

Open Access Article. Published on 15 June 2022. Downloaded on 2/7/2026 12:35:11 PM. This article is licensed under a Creative Commons Attribution-NonCommercial 3.0 Unported Licence.

alignments; as well as decreasing the HOMO energy level of conjugated polymers.[15,16] One of the most successful ways to obtain these targets is to reduce the bandgap.[17–19] Integration of donor–acceptor (D–A) functional units is one of the major ways to narrow the bandgap. Herein, the alternative donor–acceptor (D–A) copolymers have been designed. The various combinations of D–A polymers will result in completely different optoelectronic properties.

Isoindigo is commonly used as one of the strong acceptors in optoelectronics applications.[20,21] Isoindigo contains amide groups and exhibits strong π–π intermolecular interactions. Additionally, its planar π-conjugated symmetric structure results in high charge carrier mobility (~0.79 $cm^2 V^{-1} s^{-1}$).[22] The electronegative nitrogen in the compound increases more the electron affinity than a thiophene moiety.[23]

In this work, to investigate the relationships between the structure and the property of polymers when copolymers are based on the same donor but different acceptors, two D–A copolymers based on dithieno[3,2-*b*:2′,3′-*d*]pyrrole as strong donor unit and thiazole or isoindigo as acceptor units are studied. Thiazole unit is used as a weak electron-acceptor. Otherwise, isoindigo unit acts as a strong electron-acceptor. These copolymers exhibit high thermal stability; a low bandgap and excellent solubility which guarantee their potential to use in various solution-processed optoelectronic applications.

Experimental

Instruments and measurements

The chemical compositions of polymers were characterized by ^{1}H NMR spectroscopy with JEOL JNM-LA 400 FT-NMR at 25 °C. The thermal properties of small molecules were performed by using thermos-gravimetric analysis (TGA, TA Instruments, TA-250) at a heating rate of 10 °C min^{-1} under N_2. UV-vis spectrophotometer (Varian, Cary 5000) was used to measure the absorption of polymers in solution and films. 10 mg of each polymer was dissolved in 1 mL of dichlorobenzene. Thin films of samples were prepared by spin-coating on the glass substrates. The HOMO and LUMO level of the polymers were analyzed by cyclic voltammetry (ECO CHEMIE, AUTOLAB). The ordering of molecular arrangements of the thin films was confirmed by an X-ray diffractometer.

Materials

2,5-Dibromothiazole, tetrakis(triphenylphosphine)palladium(0), an-hydrous chloroform (ACS grade), anhydrous toluene (ACS grade), anhydrous tetrahydrofuran (ACS grade), were purchased from Aldrich Chemical Co., all starting materials and solvent were used without further purification unless otherwise noted. 6,6′-Dibromo-*N*,*N*′-(2-ethylhexyl)-isoindigo, 2,6-di(tributyltin)-hexyldithieno[3,2-*b*:2′,3-*d*]pyrrole were synthesized following previously published study.[21,24,25]

Synthetic routes for PDTP-IID and PDTP-Thz

Synthesis of poly{[*N*-hexyl-dithieno(3,2-*b*:2′,3′-*d*)pyrrole-2,6-diyl]*alt*-[isoindigo]} (PDTP-IID). 2,6-Di(tributyltin)-*N*-hexyldithieno[3,2-*b*:2′,3-*d*]pyrrole (0.12 g, 0.14 mmol) and 6,6′-dibromo-*N*,*N*′-(2-ethylhexyl)-isoindigo (0.09 g, 0.14 mmol) were dissolved in 10 mL of anhydrous DMF and $Pd(PPh_3)_4$ (0.017 g, 0.014 mmol) was added as the catalyst. The reaction mixture was stirred and heated under reflux at 120 °C for 24 h under a nitrogen atmosphere. After cooling, the reaction mixture was concentrated under reduced pressure and poured slowly into methanol, and stirred overnight. A dark-colored powdery solid was separated and filtered. The residue was washed with methanol and acetone for 24 h through Soxhlet extraction to remove the low molecular weight fraction of the material. After drying in a vacuum, a dark black solid of 0.098 g, 90% was obtained. Its molecular weight by GPC was M_n = 9.0 kDa; PDI = 2.10. ^{1}H NMR spectrum chemical shifts (δ, ppm): 9.05 (br, 2H), 8.17 (br, 1H), 7.37 (br, 2H), 6.77–7.00 (br, 2H), 6.3 (br, 1H), 4.1–3.4 (br, 4H), 1.91–0.83 (alkyl chains).

Synthesis of poly{[*N*-hexyl-dithieno(3,2-*b*:2′,3′-*d*)pyrrole-2,6-diyl]*alt*-[thiazole-2,5-diyl]} (PDTP-Thz). 2,6-Di(tributyltin)-*N*-hexyldithieno[3,2-*b*:2′,3-*d*]pyrrole (0.42 g, 0.5 mmol) and 2,5-dibromothiazole (0.121 g, 0.5 mmol) were dissolved in 10 mL of anhydrous DMF and $Pd(PPh_3)_4$ (30 mg, 2.5 mol%) was added as the catalyst. The reaction mixture was stirred and heated under reflux at 120 °C for 24 h under a nitrogen atmosphere. After cooling, the reaction mixture was concentrated under reduced pressure and poured slowly into methanol, and stirred overnight. A dark-colored powdery solid was separated and filtered. The residue was washed with methanol and acetone for 24 h through Soxhlet extraction to remove the low molecular weight fraction of the material. After drying in a vacuum, a dark purple solid of 0.15 g, 85% was obtained. Its molecular weight by GPC was M_n = 7.9 kDa; PDI = 1.52. The molecular structure was confirmed by ^{1}H NMR spectra in $CDCl_3$. ^{1}H NMR spectrum chemical shifts (δ, ppm): 7.90–7.80 (br, 1H), 7.0 (br, 1H), 6.60 (br, 1H), 4.05 (br, 2H), 1.78–0.91 (alkyl chains).

Devices fabrication and characterization of solar cells devices. Solar cells devices were fabricated on indium-tin-oxide (ITO)-coated glass substrates. Firstly, the glass substrates coated with indium tin oxide (ITO) were sequentially rinsed in three ultrasonic baths: acetone, de-ionized (DI) water, and isopropyl alcohol each for 10 min, respectively. Secondly, the cleaned ITO substrates were dried by putting in an oven for 24 h at 100 °C to prepare the spin-coating PEDOT:PSS which works as a hole transport layer to the backplane. After taking out the ITO from the oven, the substrates were treated with UV–ozone for 20 min. The pre-repaired PEDOT:PSS solution was sequentially spin-coated at a speed of 5000 rpm for 30 s. All mixed solutions were filtered with a 0.45 μm cellulose acetate filter before the spin-coating. Then the PEDOT:PSS film-coated ITO was annealed at 80 °C for 10 min to remove the residue solvent. The solution of polymer and PCBM (1 : 1, w/w) used as polymer emissive layer was spin-coated at 1300 rpm for 80 s on top of the PEDOT:PSS layer and subsequently annealed at 80 °C for 10 min in a glove box with nitrogen atmosphere. Calcium which is used as an electron injecting layer was deposited with a thickness of about 20 nm. The devices were completed by thermal evaporation of the Al metal cathode was carried out with a thickness of about 100 nm in a high vacuum system. All of these polymer

Open Access Article. Published on 15 June 2022. Downloaded on 2/7/2026 12:35:11 PM.
This article is licensed under a Creative Commons Attribution-NonCommercial 3.0 Unported Licence.

solar cell devices (ITO/PEDOT:PSS/polymer:PCBM/Ca/Al) were fabricated using a spin-coating method and were measured in dark and under AM 1.5 conditions from a calibrated solar simulator with an irradiation intensity of 100 mW cm^{-2} using a Keithley 236 source measure unit to define optical properties by the current–voltage (*J–V*). We fabricated 5 solar cell devices for each sample and found good reproducibility in the value of PCE.

Results and discussion

Synthesis and characterization of PDTP-IID, and PDTP-Thz

PDTP-IID and PDTP-Thz were synthesized by thermal Stille cross-coupling polymerization of 2,6-di(tributyltin)-*N*-hexyldithieno[3,2-*b*:2′,3′-*d*]pyrrole (**1**) and 6,6′-dibromo-*N*,*N*′-(2-ethylhexyl)-isoindigo or dibromothiazole (**3**) in dried anhydrous DMF under nitrogen atmosphere for 24 h. The two polymers were synthesized successfully with good yields (90% and 85%) with average molecular weights (M_n) and polydispersity index (PDI) values, respectively; and their molecular structures were confirmed by ^{1}H NMR. Two polymers exhibited good solubility in common solvents such as chloroform, THF, 1,2-dichlorobenzene, *etc.* Synthesis routes of these polymers were described in Scheme 1.

The thermal behavior of PDTP-IID, PDTP-Thz are measured by thermo-gravimetric analysis (TGA) and differential scanning calorimeter (DSC). The thermal degradation temperature (T_d) of PDTP-IID, (about 10 mg) was studied by TGA at the temperature from 30 to 600 °C at a heating rate of 10 °C min^{-1} under an N_2 atmosphere (Fig. S1a†). The polymers are dried at 60 °C under reduced pressure before measuring to remove moisture. As shown in Fig. S1a,† TGA analysis showed that the onset points of the weight loss with 5% weight loss corresponding to the melting temperature of PDTP-IID and PDTP-Thz at 230 and 280 °C, respectively, which indicated good thermal stability against oxygen.[26] No weight loss was observed before melting temperature, indicating their anhydrous nature. In the case of PDTP-Thz, the melting peak is further followed by a degradation peak, showing major weight loss starting at a temperature of about 345 °C. This results in avoiding the degradation of the active layer under applied electric fields, especially for PDTP-IID. Thus, the synthesized copolymers may be promising candidates for optoelectronic device applications. The glass transition temperature (T_g) of PDTP-IID and PDTP-Thz (5 mg) are measured by DSC in the temperature range from 30 to 400 °C at a heating rate of 10 °C min^{-1} under the atmosphere (Fig. S1b†). The copolymers PDTP-IID and PDTP-Thz exhibit T_g values at 178 and 165 °C, respectively. The value of T_g of PDTP-IID is higher than that of PDTP-Thz due to the rigid planar structure of isoindigo unit.

Optical and electrochemical properties

The UV-Vis absorptions of poly PDTP-IID and PDTP-Thz are investigated in solution (1,2-dichlorobenzene) and the solid state. Fig. 1 showed the UV-Vis absorption spectra of the copolymers PDTP-IID, PDTP-Thz obtained from their 1,2-dichlorobenzene solution and their corresponding solid-state thin films prepared by spin-coating the 1,2-dichlorobenzene solutions (10 mg/1 mL) on glass sides, respectively. The absorption maximum (λ_{max}), the onset wavelength (λ_{onset}), and the optical band gaps (E_g^{opt}) are summarized in Table 1. As displayed in Fig. 1, PDTP-IID and PDTP-Thz exhibit two major absorption peaks in the range 700–1000 nm, corresponding to intramolecular charge transfer (ICT) between the donor and acceptor group which is commonly obtained for alternating donor–acceptor copolymers.[27,28] The maximum wavelength of absorption λ_{max} of PDTP-IID and PDTP-Thz are observed at 720 and 511 nm. The extension of the absorption of PDTP-IID with

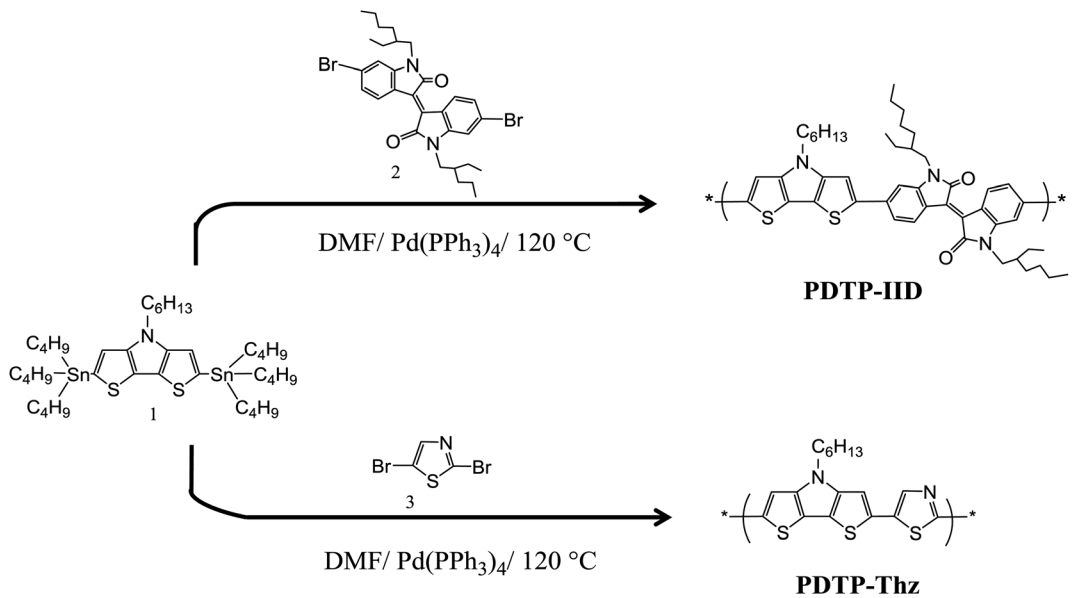

Scheme 1 General synthetic pathways for the synthesis of PDTP-IID and PDTP-Thz.

© 2022 The Author(s). Published by the Royal Society of Chemistry

Open Access Article. Published on 15 June 2022. Downloaded on 2/7/2026 12:35:11 PM.
This article is licensed under a Creative Commons Attribution-NonCommercial 3.0 Unported Licence.

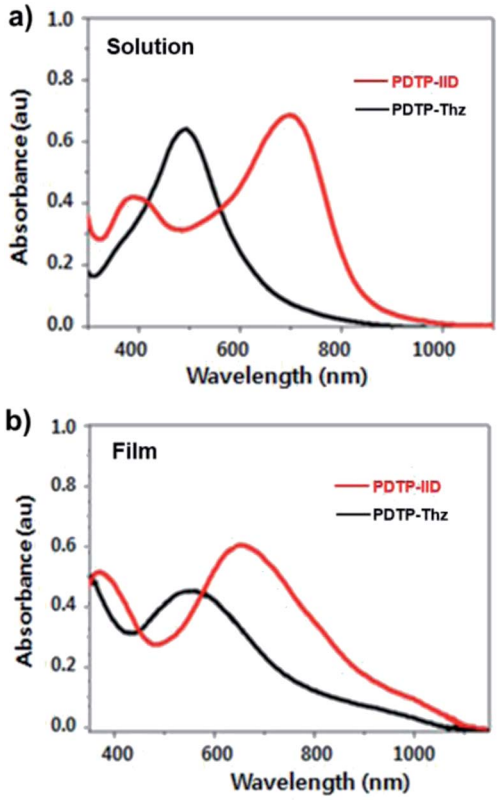

Fig. 1 UV-vis absorption spectra of PDTP-IID (red line) and PDTP-Thz (black line) in (a) dichlorobenzene and (b) as a casted film.

a longer wavelength than that of PDTP-Thz is due to a strong D–strong-A charge transfer state.[29] The UV-Vis absorption spectra in the solid state of two polymers were red-shifted about 100 nm of PDTP-IID and 120 nm of PDTP-Thz with broader absorption than their corresponding absorption in the solution due to the enhanced inter-chain interaction and molecular ordering as well as the extended π-conjugation in the solid state.[30,31] Moreover, the optical band gaps of all polymers which are determined from λ_{onset} [E_g^{opt} (eV) = 1240/λ_{onset} (nm)] are lower in thin films than in solution. The optical band gap of PDTP-IID and PDTP-Thz are 1.29 and 1.51 eV, respectively. Two polymers exhibit a broad absorption range (700–1000 nm) with a low bandgap; we believe that it will improve the light-harvesting capacity and the photocurrent of the devices.

The electrochemical properties of copolymer PDTP-IID and PDTP-Thz are studied to investigate the redox behavior and to determine the position of their highest occupied molecular orbital (HOMO) and lowest unoccupied molecular orbital (LUMO). The cyclic voltammetry (CV) of the PDTP-IID and PDTP-Thz are displayed in Fig. 2 and the revealed CV data (HOMO and LUMO levels, as well as electrochemical bandgap energy (E_g^{ec})), are summarized in Table 1. In the anodic scan, the onset of oxidation occurred at 1.10 eV of PDTP-IID and 0.72 eV of PDTP-Thz. The highest occupied molecular orbital (HOMO) energy levels of PDTP-IID and PDTP-Thz are estimated to be −5.49 and −5.11 eV. In the cathodic scan, the onset of reduction occurred at −0.78 for PDTP-IID and −0.89 for PDTP-Thz. The lowest unoccupied molecular orbital (LUMO) energy levels of PDTP-IID and PDTP-Thz are estimated to be −3.61 and −3.50 eV. The energy band gap of PDTP-IID and PDTP-Thz which were calculated from the difference between E_{HOMO} and E_{LUMO} are 1.88 and 1.61 eV as shown in Table 1, respectively. All HOMO energy levels of two polymers were found to be below the air oxidation (*ca.* −5.27 eV) which shows good stability against air and oxygen. It is one of the most important factors in considerations of device application. The estimated E_g^{ec} values for polymers are higher than the corresponding values for E_g^{opt}. The reason might lie in the interface barrier present between the polymer film and the electrode surface.

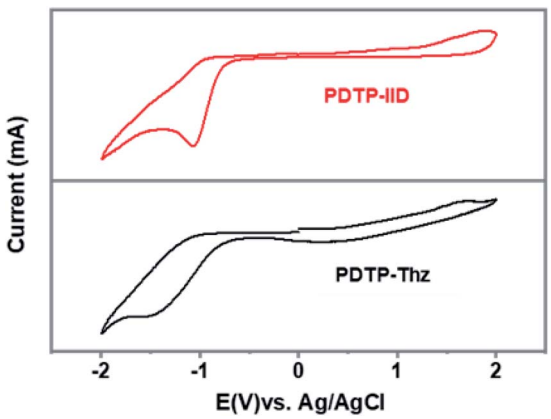

Fig. 2 Cyclic voltammogram (electrolyte: 0.1 M Bu_4NClO_4 in acetonitrile scan rate: 50 mV s^{-1}, reference electrode: Ag/AgCl).

Table 1 Optical and electrochemical properties of PDTP-IID and PDTP-Thz

	UV-vis absorption				Cyclic voltammetry		
	Solution[b]	Film					
Polymer[a]	λ_{max} (nm)	λ_{max} (nm)	λ_{onset} (nm)	E_g^{optc} (eV)	HOMO (eV)	LUMO (eV)	E_g^{ecd} (eV)
PDTP-IID	720	700	962	1.29	−5.49	−3.61	1.88
PDTP-Thz	511	520	820	1.51	−5.11	−3.50	1.61

[a] All polymers were collected *via* Stille-coupling. [b] Samples were prepared from 1,2-dichlorobenzene solution. [c] Optical band gap E_g^{opt} was calculated from using the onset of the UV-Vis spectrum ($E_g^{opt} = 1240/\lambda_{onset}$). [d] Electrical band gap E_g^{ec} was calculated from $E_g^{ec} = E_{LUMO} - E_{HOMO}$.

© 2022 The Author(s). Published by the Royal Society of Chemistry

Open Access Article. Published on 15 June 2022. Downloaded on 2/7/2026 12:35:11 PM.
This article is licensed under a Creative Commons Attribution-NonCommercial 3.0 Unported Licence.

Solid-state properties

In BHJ solar cells, the surface morphology of the active layer is very important to their photovoltaic performance. To determine the surface of the film from copolymers, from blends of the copolymers:$PC_{61}BM$ and blends of the copolymers:$PC_{71}BM$ in 1 : 1 ratio in 1,2-dichlorobenzene, tapping-mode atomic force microscopy (AFM) is used. The surface roughness of polymers and polymer–fullerene blending films are measured by atomic force microscopy (AFM) in non-contact mode. The samples were prepared by spin coating a 10 mg mL^{-1} solution at 1000 rpm for 30 s in anhydrous 1,2-dichlorobenzene on the ITO glass. Fig. 3 shows the three-dimensional topographic images of polymers and polymer–fullerene blending films, respectively. The surface roughness values of copolymers PDTP-IID and PDTP-Thz from topography images are 4.06 and 3.03 nm in root mean square (rms), respectively. Different morphologies of these polymers suggest that the interaction between the molecules of each polymer is different. The RMS roughness (R_q) of PDTP-IID:$PC_{61}BM$, PDTP-Thz:$PC_{61}BM$, and PDTP-IID:$PC_{71}BM$, PDTP-Thz:$PC_{71}BM$ films are 3.81, 0.79 and 2.94, 0.69 nm, respectively. After blending with fullerene, the surface roughness of the blend of PDTP-IID and PDTP-Thz is decreased compared to the surface roughness of films without fullerene. However, the blends of PDTP-IID:$PC_{71}BM$ and PDTP-Thz:$PC_{71}BM$ films exhibit a smoother surface than that of PDTP-IID:$PC_{61}BM$ and PDTP-Thz:$PC_{61}BM$. The smoother surface for the copolymers indicated that the miscibility between the copolymers and $PC_{71}BM$ is better than that of the copolymers and $PC_{61}BM$ which resulted in increased J_{SC} and FF.[32]

The structural ordering of PDTP-IID and PDTP-Thz are also investigated by X-ray diffraction measurement. The samples were prepared by spin coating a 10 mg mL^{-1} solution in anhydrous 1,2-dichlorobenzene on the glass substrates. As observed in XRD data (Fig. 4), PDTP-IID exhibited a strong diffraction peak at $2\theta = 5.4°$ which reflects distances between main backbones separated by alkyl chains.[21] While PDTP-Thz showed a clear diffraction peak at $2\theta = 23.4°$ corresponding to π–π stacking between molecules.

Polymer solar cells device performance

To investigate the photovoltaic properties of PDTP-IID and PDTP-Thz, the bulk heterojunction polymer solar cells (PSCs) were fabricated with a structure of ITO/PEDOT:PSS/polymers:PCBM (1 : 1, w/w)/Ca/Al (Scheme 2). The optimized results were obtained by varying polymer:PCBM weight ratios and the thickness of the active layer.[33,34] The optimized thickness of the active layer for all polymers:PCBM was around 80 nm. In these devices, the copolymers worked as donors and PCBM worked as an acceptor. 1,2-Dichlorobenzene was used as a solvent to get good blending films of the copolymers and PCBM. Fig. 5 shows the *I–V* curve of the photovoltaic device under the illumination of AM 1.5, 100 mW cm^{-2}. The corresponding V_{OC}, short-circuit current (J_{SC}), fill factor (FF) and PCE of the devices are summarized in Table 2.

The V_{OC} of the device based on PDTP-IID with PCBM are 0.43 and 0.37 V which is higher than that of the device based on PDTP-Thz with PCBM because PDTP-IID exhibits the deeper HOMO level of the donor. Furthermore, the difference between the HOMO of the donor (copolymers) and the LUMO level of the acceptor (PCBM) is closely related to the open-circuit voltage V_{OC} values of the resulting polymers solar cells. PDTP-IID exhibits a HOMO level of −5.49 eV meanwhile PDTP-Thz exhibits a HOMO level of −5.11 eV.

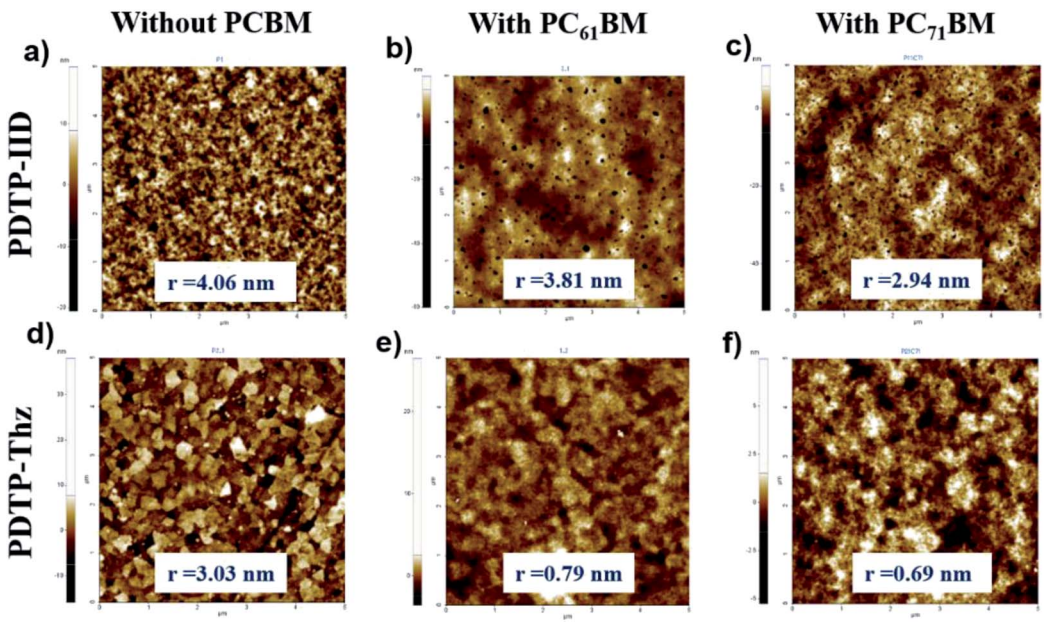

Fig. 3 Topography of AFM images (5 × 5 μm^2) of the active films prepared by (a, d) PDTP-IID and PDTP-Thz without PCBM; (b, e) PDTP-IID and PDTP-Thz with $PC_{61}BM$ and (c, f) PDTP-IID and PDTP-Thz with $PC_{71}BM$.

© 2022 The Author(s). Published by the Royal Society of Chemistry

Open Access Article. Published on 15 June 2022. Downloaded on 2/7/2026 12:35:11 PM.
This article is licensed under a Creative Commons Attribution-NonCommercial 3.0 Unported Licence.

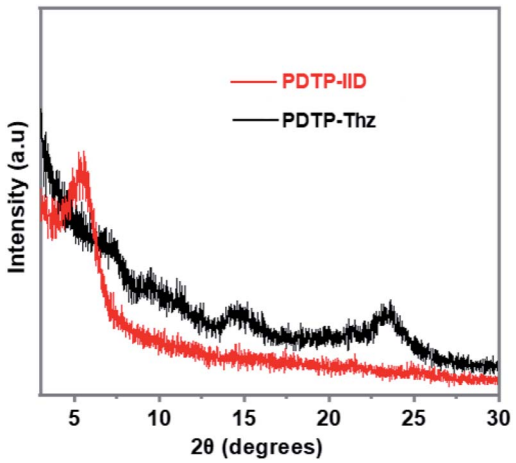

Fig. 4 X-ray diffraction patterns of PDTP-IID and PDTP-Thz.

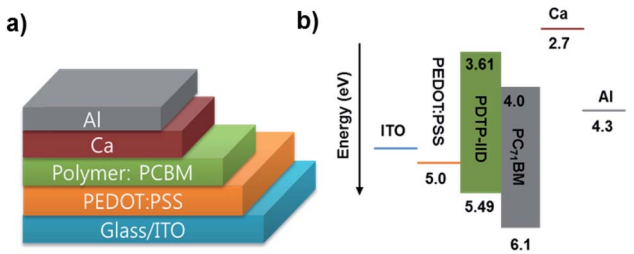

Scheme 2 (a) Schematic architecture of fabricated bulk-heterojunction (BHJ) polymer solar cells, (b) the presentative of energy band diagram of charge transport when PDTP-IID:$PC_{71}BM$ is used.

Moreover, the short-circuit current density (J_{SC}) also affects the efficiency of the device. Although the device based on PDTP-IID as donor and $PC_{61}BM$ or $PC_{71}BM$ as an acceptor, they obtained higher high short-circuit current density (J_{SC}) than those of the device based on PDTP-Thz as donor and $PC_{61}BM$ or $PC_{71}BM$ as an acceptor. The main reason is due to the photon

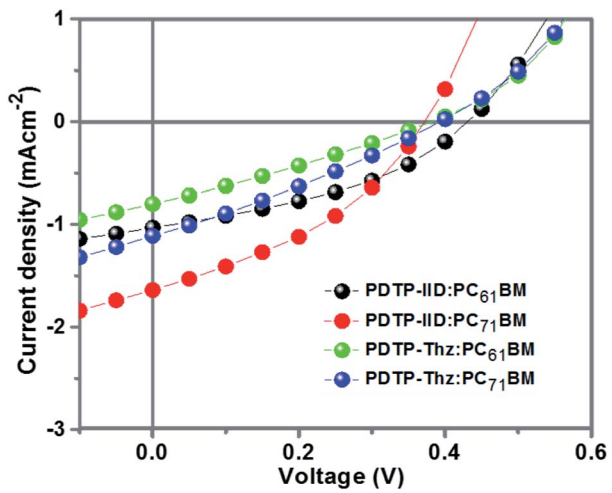

Fig. 5 *I–V* curves of the PSCs based on PDTP-IID and PDTP-Thz under illumination of AM 1.5 G, 100 mW cm^{-2}.

Table 2 Device characteristics of PSCs based on PDTP-IID and PDTP-Thz polymers with $PC_{61}BM$ and $PC_{71}BM$

Polymer:PCBM (1 : 1)	V_{OC} (V)	J_{SC} (mA cm^{-2})	FF	PCE (%)
PDTP-IID:$PC_{61}BM$	0.43	1.03	0.39	0.17
PDTP-Thz:$PC_{61}BM$	0.38	0.80	0.28	0.09
PDTP-IID:$PC_{71}BM$	0.37	1.64	0.38	0.23
PDTP-Thz:$PC_{71}BM$	0.39	1.11	0.29	0.13

absorption properties of PDTP-IID in the wide-range wavelength which is better than that of PDTP-Thz. This results PDTP-IID can absorb more light than PDTP-Thz.

Compared to the device based on the copolymers with a different type of PCBM, the device containing $PC_{71}BM$ as an acceptor exhibited a higher short-circuit current density of 1.64 mA cm^{-2} of PDTP-IID:$PC_{71}BM$ and 1.11 mA cm^{-2} of PDTP-Thz:$PC_{71}BM$ leading to the better performance (maximum PCE of 0.23% of PDTP-IID:$PC_{71}BM$ and 0.13% of PDTP-Thz:$PC_{71}BM$) than device containing $PC_{61}BM$ as an acceptor (maximum PCE of 0.17% of PDTP-IID:$PC_{61}BM$ and 0.09% of PDTP-Thz:$PC_{61}BM$). The miscibility between the copolymers and $PC_{71}BM$ is better than that of the copolymers and $PC_{61}BM$. So, the surface of PDTP-IID:$PC_{71}BM$ and PDTP-Thz:$PC_{71}BM$ films are smoother than that of PDTP-IID:$PC_{61}BM$ and PDTP-Thz:$PC_{61}BM$ which leads to increased J_{SC} and FF (Table 2). Besides, $PC_{71}BM$ has similar electronic properties as PCBM but a higher absorption coefficient in the visible region which can compensate for the poor absorption of the polymers in this range.[35]

Conclusions

Two new π-conjugated copolymers, PDTP-IID and PDTP-Thz were successfully synthesized with good yields. These copolymers showed good thermal stability which is suitable for optoelectronic devices. Due to the electron-withdrawing ability of isoindigo unit, the copolymer PDTP-IID exhibited a narrower optical band gap (1.29 eV) and a lower-lying HOMO energy level (−5.49 eV) than that of the copolymer PDTP-Thz (1.51 eV). Solid states properties of PDTP-IID and PDTP-Thz were confirmed by AFM and XRD measurements. After blending with fullerene, the surface roughness was decreased. Especially, the RMS roughness of blending films made from PDTP-IID:$PC_{71}BM$ and PDTP-Thz:$PC_{71}BM$ were improved and exhibited smoother surfaces than that of PDTP-IID:$PC_{61}BM$ and PDTP-Thz:$PC_{61}BM$ blending films. Although these devices based on these polymers did not exhibit high efficiency, we still can confirm that the photovoltaic performance of the polymers combined *N*-alkyl dithieno[3,2-*b*:2′,3′-*d*]pyrroles-based donor and strong acceptor was better than that of the polymers based on strong donor and weak acceptor. These copolymers are promising candidate materials for developing new materials in optoelectronic applications.

Author contributions

C. K. Trinh: conceptualization, methodology, formal analysis, investigation, visualization, writing – original draft, review &

Open Access Article. Published on 15 June 2022. Downloaded on 2/7/2026 12:35:11 PM. This article is licensed under a Creative Commons Attribution-NonCommercial 3.0 Unported Licence.

editing, resources. G. M. Nassar: investigation, methodology. N. I. Abdo: writing – review & editing. S. Jung: formal analysis. W. Kim: formal analysis. Supervisor K. Lee: writing – review & editing, supervision. Supervisor J.-S. Lee: writing – review & editing, resources, supervision.

Conflicts of interest

There are no conflicts to declare.

Acknowledgements

We would like to thank Van Lang University, Vietnam for the support for this research.

Notes and references

1 M. V. Srinivasan, N. Tsuda, P.-K. Shinc and S. Ochiai, *RSC Adv.*, 2015, **5**, 56262–56269.
2 Y. Zhang, X. Li, T. Dai, D. Xu, J. Xi and X. Chen, *RSC Adv.*, 2019, **9**, 24895–24903.
3 M. Shaker, C. K. Trinh, W. Kim, H. Kim, K. Lee and J.-S. Lee, *New J. Chem.*, 2015, **39**, 4957–4964.
4 A. A. El-Shehawy, N. I. Abdo, A. A. El-Barbary, J. Choi, H. S. El-Sheshtawy and J.-S. Lee, *J. Mater. Sci. Nanomater.*, 2018, **2**(1), 1000103–1000111.
5 M. Goel, C. D. Heinrich, G. Krauss and M. Thelakkat, *Macromol. Rapid Commun.*, 2019, 1800915–1800944.
6 S. Song, Y. Jin, S. Park, S. Cho, I. Kim, K. Lee, A. J. Heeger and H. Suh, *J. Mater. Chem.*, 2010, **20**, 6517–6523.
7 N. Yao, J. Wang, Z. Chen, Q. Bian, Y. Xia, R. Zhang, J. Zhang, L. Qin, H. Zhu, Y. Zhang and F. Zhang, *J. Phys. Chem. Lett.*, 2021, **12**(20), 5039–5044.
8 L. Hu, W. Qiao, J. Qi, X. Zhang, J. Han and C. Wang, *RSC Adv.*, 2016, **6**, 22494–22499.
9 S. J. Evenson, M. E. Mulholland, T. E. Anderson and S. C. Rasmussen, *Asian J. Org. Chem.*, 2020, **9**, 1–8.
10 E. J. Zhou, M. Nakamura, T. Nishizawa, Y. Zhang, Q. S. Wei, K. Tajima, C. H. Yang and K. Hashimoto, *Macromolecules*, 2008, **41**, 8302–8305.
11 Y. Geng, J. Cong, K. Tajima, Q. Zeng and E. Zhou, *Polym. Chem.*, 2014, **5**, 6797–6803.
12 W. Lee, G. H. Kim, E. Jeong, X. Wang, S. Yum, S. J. Ko, S. Hwang, J. Y. Kim and H. Y. Woo, *Macromol. Chem. Phys.*, 2013, **214**, 2083–2090.
13 W. Yue, Y. Zhao, S. Y. Shao, H. K. Tian, Z. Y. Xie, Y. H. Geng and F. S. Wang, *J. Mater. Chem.*, 2009, **19**, 2199–2206.
14 E. J. Zhou, S. P. Yamakawa, K. Tajima, C. H. Yang and K. Hashimoto, *Chem. Mater.*, 2009, **21**, 4055–4061.
15 J. Zhang, L. Wang, C. Jiang, B. Cheng, T. Chen and J. Yu, *Adv. Sci.*, 2021, **8**, 2102648–2102658.
16 E. U. Rashid, J. Iqbal, M. I. Khan, Y. A. El-Badry, K. Ayub and R. A. Khera, *RSC Adv.*, 2022, **12**, 12321–12334.
17 D. Hashemi, X. Ma, J. Kim and J. Kieffer, *Phys. Chem. Chem. Phys.*, 2019, **21**, 789–799.
18 W. Chen, W. Shen, H. Wang, F. Liu, L. Duan, X. Xu, D. Zhu, M. Qiu, E. Wang and R. Yang, *Dyes Pigm.*, 2019, **166**, 42–48.
19 M. C. Scharber and N. S. Sariciftci, *Adv. Mater. Technol.*, 2021, **6**, 2000857–2000864.
20 C. K. Trinh, H.-J. Lee, J. W. Choi, M. Shaker, W. Kim and J.-S. Lee, *New J. Chem.*, 2018, **42**, 2557–2563.
21 W. Elsawy, C.-L. Lee, S. Cho, S.-H. Oh, S.-H. Moon, A. Elbarbary and J.-S. Lee, *Phys. Chem. Chem. Phys.*, 2013, **15**, 15193–15203.
22 T. Lei, Y. Cao, Y. Fan, C.-J. Liu, S.-C. Yuan and J. Pei, *J. Am. Chem. Soc.*, 2011, **133**(16), 6099–6101.
23 E. Zaborova, P. Cháveza, R. Becharab, P. Lévêqueb, T. Heiserb, S. Méryc and N. Leclerc, *Chem. Commun.*, 2013, **49**, 9938–9940.
24 Y. J. Park, J. H. Seo, W. Elsawy, B. Walker, S. Cho and J.-S. Lee, *J. Mater. Chem. C*, 2015, **3**, 5951–5957.
25 S. J. Evenson, M. J. Mumm, K. I. Pokhodnya and S. C. Rasmussen, *Macromolecules*, 2011, **44**(4), 835–841.
26 X. Liu, C. Zhang, S. Pang, N. Li, C. J. Brabec, C. Duan, F. Huang and Y. Cao, *Front. Chem.*, 2020, **8**, 302, DOI: **10.3389/fchem.2020.00302h**.
27 Y. Zhu, R. D. Champion and S. A. Jenekhe, *Macromolecules*, 2006, **39**, 8712–8719.
28 F. Huang, K.-S. Chen, H.-L. Yip, S. K. Hau, O. Acton, Y. Zhang, J. Luo and A. K.-Y. Jen, *J. Am. Chem. Soc.*, 2009, **131**, 13886–13887.
29 F. Grenier, P. Berrouard, J.-R. Pouliot, H.-R. Tseng, A. J. Heeger and M. Leclerc, *Polym. Chem.*, 2013, **4**, 1836–1841.
30 L. Liao, L. Dai, A. Smith, M. Durstock, J. Lu, J. Ding and Y. Tao, *Macromolecules*, 2007, **40**(26), 9406–9412.
31 T. H. Lee, D. H. Kim, E. J. Lee and D. K. Moon, *J. Ind. Eng. Chem.*, 2018, **65**, 195–204.
32 C. Sartorio, V. Campisciano, C. Chiappara, S. Cataldo, M. Scopelliti, M. Gruttadauria, F. Giacalone and B. Pignataro, *J. Mater. Chem. A*, 2018, **6**, 3884–3894.
33 M. Shaker, J.-H. Lee, C. K. Trinh, W. Kim, K. Lee and J.-S. Lee, *RSC Adv.*, 2015, **5**, 66005–66012.
34 D. Cortizo-Lacalle, C. T. Howells, U. K. Pandey, J. Cameron, N. J. Findlay, A. R. Inigo, T. Tuttle, P. J. Skabara and I. D. W. Samuel, *Beilstein J. Org. Chem.*, 2014, **10**, 2683–2695.
35 B. Wang, Y. Fu, C. Yan, R. Zhang, Q. Yang, Y. Han and Z. Xie, *Front. Chem.*, 2018, **6**, 198, DOI: **10.3389/fchem.2018.00198**.

© 2022 The Author(s). Published by the Royal Society of Chemistry